# The Origin of Switchbacks in the Solar Corona: Linear Theory

G. P. Zank[1,2] , M. Nakanotani[1] , L.-L. Zhao[1] , L. Adhikari[1] , and J. Kasper[3]

[1] Center for Space Plasma and Aeronomic Research (CSPAR), University of Alabama in Huntsville, Huntsville, AL 35805, USA
[2] Department of Space Science, University of Alabama in Huntsville, Huntsville, AL 35899, USA
[3] Department of Climate and Space Sciences and Engineering, University of Michigan, 2455 Hayward Street, Ann Arbor, MI 48109-2143, USA

## Abstract

The origin, structure, and propagation characteristics of a switchback are compelling questions posed by Parker Solar Probe (PSP) observations of velocity spikes and magnetic field reversals. By assuming interchange reconnection between coronal loop and open magnetic field, we show that this results in the generation of upward (into the heliosphere) and downward complex structures propagating at the fast magnetosonic speed (i.e., the Alfvén speed in the low plasma beta corona) that can have an arbitrary radial magnetic field deflection, including "S-shaped." We derive the evolution equation for the switchback radial magnetic field as it propagates through the inhomogeneous supersonic solar corona. An analytic solution for arbitrary initial conditions is used to investigate the properties of a switchback propagating from launch $\sim$6 to $\sim$35 $R_\odot$ where PSP observed switchbacks during its first encounter. We provide a detailed comparison to an example event, showing that the magnetic field and plasma solutions are in accord with PSP observations. For a simple single switchback, the model predicts either a single or a double-humped structure; the former corresponding to PSP observing either the main body or the flanks of the switchback. The clustering of switchbacks and their sometimes complicated structure may be due to the formation of multiple closely spaced switchbacks created by interchange reconnection with numerous open and loop magnetic field lines over a short period. We show that their evolution yields a complex, aggregated group of switchbacks that includes "sheaths" with large-amplitude radial magnetic field and velocity fluctuations.

*Unified Astronomy Thesaurus concepts:* Active solar corona (1988); Solar coronal waves (1995); Interplanetary turbulence (830)

## 1. Introduction

Structures described as "switchbacks" were observed by the Parker Solar Probe (PSP) during its first (Kasper et al. 2019) and subsequent encounters with the Sun and extended solar corona. Switchbacks were identified initially as solar wind jumps in the plasma flow and a magnetic field orientation that changed by at least 45° from the background field and then returned to the background orientation during an interval of ⩾10 s (Kasper et al. 2019). Perhaps the most detailed and revealing analysis of the observed properties of switchbacks is by Dudok de Wit et al. (2020). Dudok de Wit et al. (2020) examined two statistical properties of the PSP magnetic field observations in classifying switchbacks: (1) the distribution of normalized magnetic field deflections and (2) waiting times (the time between the end of an event and the onset of the next). Based on (1), Dudok de Wit et al. (2020) found that the distribution of magnetic field deflections is essentially continuous and monotonically decreasing toward 180° reversals (the least numerous but most extreme deflections), suggesting that there does not exist a typical range of deflections that defines a switchback. However, the waiting time and residence time distributions indicate the existence of two solar wind states. One corresponds to a quiescent regime associated with a more pristine solar wind possessing turbulent fluctuations with relatively small deflections and "short memory." The second is a wind in which sometimes sizable deflections tend to aggregate and possess "long memory," indicating that the switchback distribution is statistically distinct from turbulence in the quiescent solar wind despite switchbacks having a continuous range of deflections. Dudok de Wit et al. (2020) concluded that the quiescent solar wind and associated "memory-less" turbulence originates from low in

corona, "well below the Alfvén surface," whereas switchbacks possess a distinct origin higher in the solar corona. The origin of a quiescent solar wind and memory-less turbulence is consistent with the idea that quasi-2D turbulence is generated in the photosphere with the dynamical emergence of the magnetic carpet and the heating of the solar corona via turbulent dissipation (Zank et al. 2018; Adhikari et al. 2020a, 2020b).

The origin of switchbacks has not been established and several ideas have been advanced. These models tend to be related to either magnetic reconnection (Yamauchi et al. 2004; Fisk & Kasper 2020) or large-amplitude Alfvén waves (Matteini et al. 2014, 2015; Tenerani et al. 2020). Indeed, when writing this paper, we learned of the work of Fisk & Kasper (2020) that, in some respects, closely parallels ours conceptually although the quantitative analysis here is very different. The reconnection model of Yamauchi et al. (2004) posits that emerging closed magnetic flux from the photosphere may reconnect with an open magnetic field to produce a propagating kink. Fisk & Kasper (2020) suggest a similar mechanism but instead exploiting interchange reconnection of large-scale coronal loops and open field as part of the global circulation that drags magnetic field around in the corona. The argument leveled against both these ideas for the formation of switchbacks (Fisk & Schwadron 2001; Fisk 2005; Tenerani et al. 2020) was that the open magnetic field would relax and straighten in the low plasma beta corona to maintain constant magnetic pressure in the corona (Fisk 2005; Landi et al. 2006; Tenerani et al. 2020). However, this argument holds only if the propagating structure is an incompressible Alfvénic structure. This is because the fastest magnetohydrodynamic (MHD) mode in the system, the fast magnetosonic mode, will
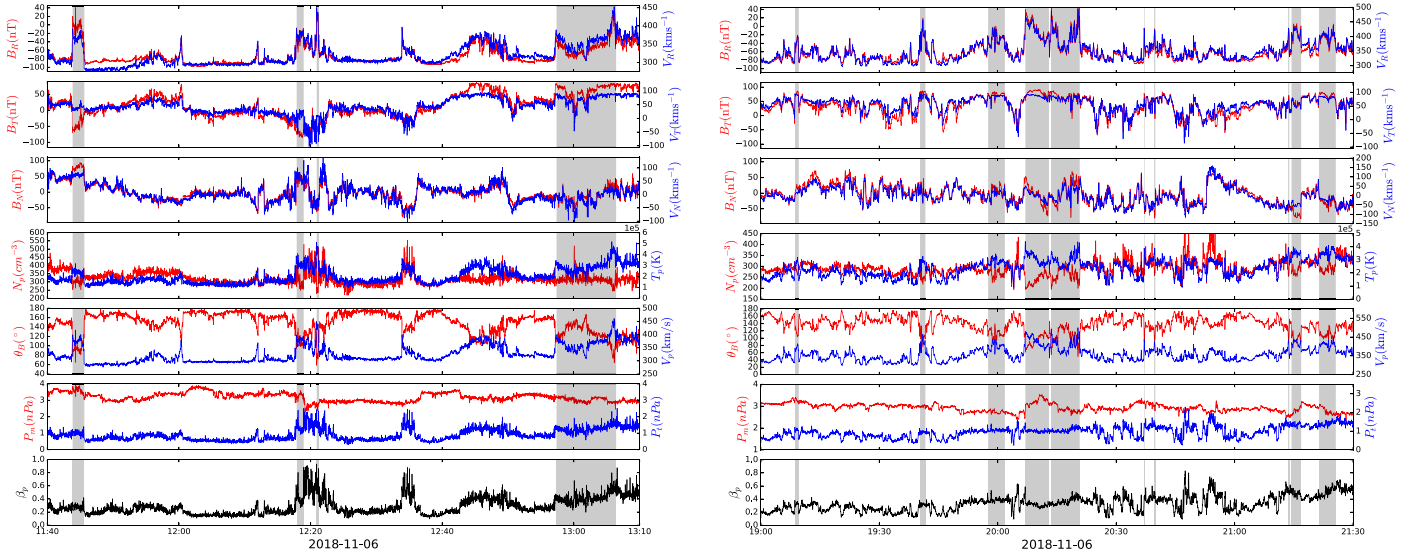
**Figure 1.** Plasma variables, shown in the RTN coordinate system, observed by PSP during the first encounter from 11:40–13:20 (left panel) to 19:00–21:40 UT (right) on 2018 November 6. In descending order, the panels show the radial magnetic field $B_R$ and velocity component $V_R$, the tangential magnetic field $B_T$ and velocity component $V_T$, the normal magnetic field $B_N$ and velocity component $V_N$, the proton number density $n_p$ and temperature $T_p$, the angle $\theta_B$, which is the angle between $\boldsymbol{B}$ and the radial direction, and the flow speed $V_p = |\boldsymbol{V}|$, the thermal proton pressure $P_t = n_p k_B T_P$ and magnetic pressure $P_m = B^2/2\mu_0$, and the proton plasma beta $\beta$. The shaded gray bars identify switchbacks based on the criteria listed in the text.

straighten the magnetic field ahead of the slower propagating Alfvén mode.

In a low plasma beta corona, it is difficult to distinguish the fast magnetosonic mode from an Alfvén wave since the propagation speed for both is essentially the Alfvén speed. However, the Alfvén wave propagates along the mean magnetic field $\boldsymbol{B}$, whereas the fast mode with phase speed $V_f \simeq V_A$ propagates at all angles relative to $\boldsymbol{B}$. Plotted in Figure 1 is PSP plasma (Solar Wind Electrons Alphas and Protons (SWEAP); Kasper et al. 2016) and magnetic field (Electromagnetic Fields Investigation (FIELDS); Bale et al. 2016) data from 11:40–13:20 to 19:00–21:40 UT on 2018 November 6, respectively, from the first PSP encounter (Kasper et al. 2019). A set of "obvious" switchbacks is identified by the gray bars. By obvious switchbacks, we mean those structures that were identified by (1) a magnetic field that rotated more than 45° from the quiet state and (2) an event that was of at least 10 s duration (Kasper et al. 2019). We emphasize that these criteria probably exclude most switchbacks if one adopts the statistical definition of Dudok de Wit et al. (2020).

To more clearly illustrate the character of these more extreme switchbacks, we plot in Figure 2 an expanded view of the switchback observed from ∼11:43 to 11:46 on 2018 November 6. Although we have no particularly good reason for choosing this over another, it is a rather clean example. Figure 2 includes a panel showing the angle made by the mean magnetic field with the radial direction $\theta_B$. The plot of $\theta_B$ indicates that the field is essentially anti-aligned with the radial solar wind flow. As illustrated in the top three panels of Figure 2, the switchback exhibits both $B_{\parallel}$ and $B_{N,T}$ variation. This is not Alfvénic in character—$B_{\parallel}$ variation is the defining signature of fast magnetosonic modes (e.g., Lighthill 1960). Notice too that the parallel (radial) magnetic field and velocity are correlated—again, this is not an Alfvénic but a magnetosonic characteristic. There is some correlation between the transverse magnetic fields and velocities in the switchback, but such a correlation holds for magnetosonic modes in the small plasma beta limit (see the Appendix for the fast magnetosonic

eigenvalues in the $\beta_p \ll 1$ limit). A further important point is that despite the correlations, the switchback of Figure 2 exhibits neither simple linear magnetosonic nor linear Alfvénic correlations indicating that a switchback is neither a linear magnetosonic wave not a linear Alfvén wave. However, because of the $B_{\parallel}$ and parallel velocity variation within a switchback, switchbacks are unequivocally not Alfvénic in character. This should not be surprising if we accept the origin of switchbacks as being due to the interchange reconnection mechanism advocated here since compression is likely to be a feature of the initial state. This and the identified switchbacks in Figure 1 are characterized by changes in the proton number density, pressure, and temperature, all of which should not vary in an Alfvénic structure. Indeed, since switchbacks exhibit expressly compressive characteristics, they can be regarded as complex structures that propagate at the fast magnetosonic speed rather than Alfvénic structures. The structure of switchbacks is determined by the initial conditions and the subsequent evolution of that data. Finally, switchbacks are observed to be outwardly propagating structures (Kasper et al. 2019).

As noted above, our idea for the origin of switchbacks is conceptually similar to that advocated by Fisk & Kasper (2020) and consistent with the contention by Dudok de Wit et al. (2020) that switchbacks originate from higher up in the corona rather than just above the photosphere. A cartoon illustrating our conceptual picture of the origin of switchbacks is illustrated in Figure 3. Figure 3(a) shows a large coronal loop, which has a characteristic height of ∼6 $R_\odot$ typically, close to a region of open magnetic field that extends into the supersonic solar wind. Both the loop and the open field region are comprised of multiple "field lines," which is important in view of the observed (statistical) clustering of switchbacks (Dudok de Wit et al. 2020). The random walk of the magnetic field footpoints will sometimes bring the oppositely oriented open magnetic fields and loop magnetic fields sufficiently close to induce multiple successive closely spaced (spatially and temporally) interchange reconnection events as illustrated in Figures 3(b) and (c). Multiple interchange reconnection events will occur
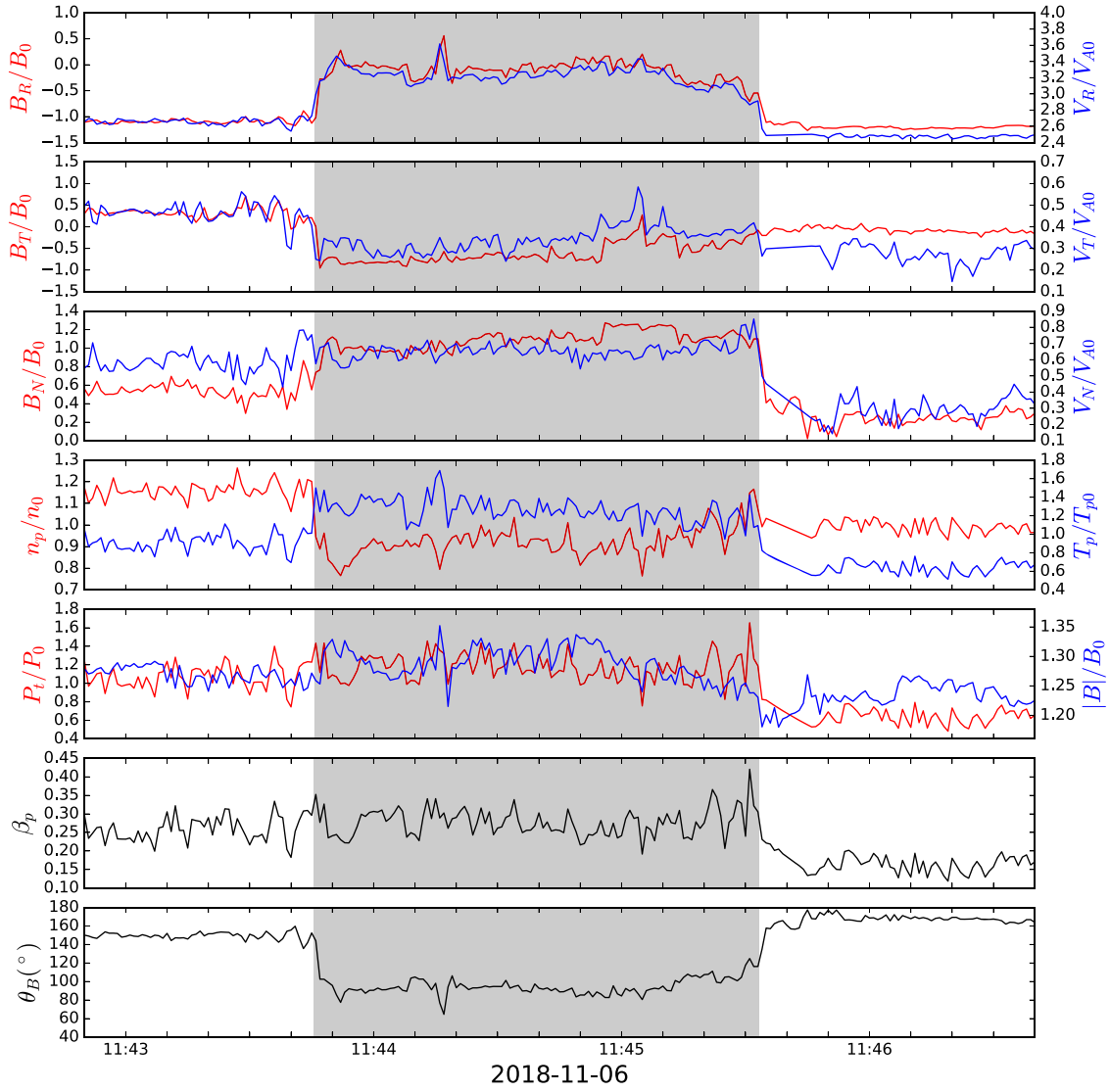
**Figure 2.** Expanded view of the plasma variables, now shown in normalized variables, observed by PSP during the first encounter from 11:43−11:46 on 2018 November 6. In descending order, the panels show the radial magnetic field $B_R/B_0$ and velocity component $V_R/V_{A0}$ normalized to the mean magnetic field strength $B_0$ and Alfvén speed $V_{A0}$ ahead of the switchback, the normalized transverse magnetic field $B_T/B_0$ and velocity component $V_T/V_{A0}$, the normalized magnetic field $B_N/B_0$ and velocity component $V_N/V_{A0}$, the normalized proton number density $n_p/n_0$, thermal pressure $P_t/P_0$ and temperature $T_p/T_0$, where $n_0$, $P_0$, and $T_0$ are the mean number density, pressure, and temperature just ahead of the switchback. The angle $\theta_B$ is the angle between $\boldsymbol{B}$ and the radial direction. The thermal proton pressure $P_t = n_p k_B T_P$ and $\beta_p$ is the proton plasma beta.

while the open field and loop regions converge, ending only when (1) flux from either of the regions is annihilated, or (2) footpoint motions drag the two regions apart. The finite time over which multiple interchange reconnection events occur will lead to a clustering of the switchback events. As illustrated in Figures 3(b) and (c), "S-shaped" structures, as well as less extreme deviations, will be launched on the open field both radially upward and downward as a result of an individual interchange reconnection event. Of course, a range of possible magnetic field deflections can be launched by this mechanism and not just extreme S-shaped examples. Furthermore, the local region of reconnected magnetic field will exhibit a perturbation or change in amplitude as well since the initially open and loop field lines will have different strengths. Besides a perturbed magnetic field, hot tenuous loop plasma will be released by the interchange reconnection event, most likely in the form of a jet propagating at the Alfvén speed relative to the background solar wind flow and in a direction that is not necessarily radial.

The initial switchback launched by such an event will therefore be a structure comprised of a perturbed magnetic field in both the radial and transverse magnetic field, velocity, and likely entrains hot tenuous gas that is different from the surrounding ambient plasma.

The release of hot tenuous loop plasma into the lower regions of the corona via multiple reconnection events is a possible heating source that may drive the slow solar wind or further drive the fast solar wind, and is related to ideas advocated by Fisk et al. (1999) and Fisk (2003).

Small amplitude waves are apparent in Figures 1 and 2, both outside and inside switchbacks. These have been investigated in some detail by Zhao et al. (2020) and McManus et al. (2020). Zhao et al. (2020) found that the cross helicity is predominantly positive near the first perihelion, indicating outwardly propagating waves. The wave propagation direction turns inward temporarily within switchbacks, but the propagation direction with respect to the local background magnetic
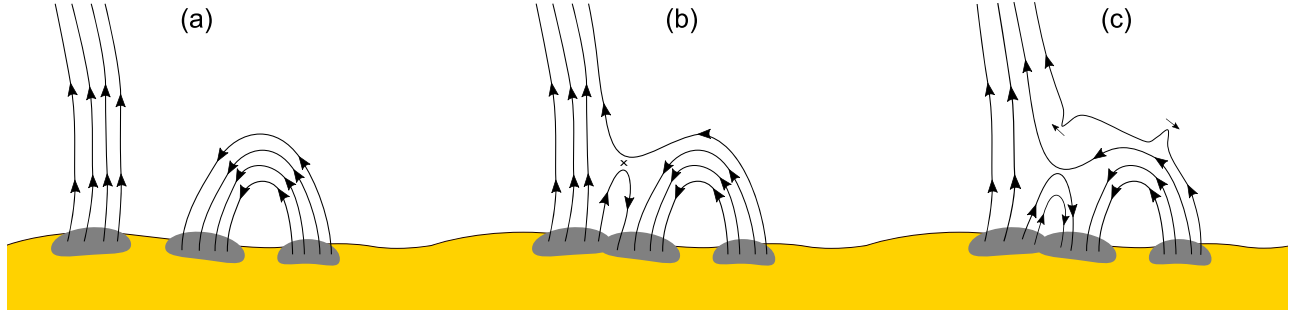
**Figure 3.** (a) Cartoon showing the time sequence of interchange reconnection events between a coronal loop and open magnetic field lines, starting with them separated (a). Part (b) shows the first of the interchange reconnection events producing a reconfigured open field line with an approximately S-shaped structure and a new smaller closed loop. Part (c) illustrates the launch of the nominal switchback, with one propagating upward and the other downward toward the solar surface in the sub-Alfvénic coronal flow. In (c), a second interchange reconnection event is occurring and will produce a subsequent set of switchbacks propagating up and down as before.

field does not change. Using a local mean magnetic field Horbury et al. ([2008](#)) and McManus et al. ([2020](#)) defined a "rectified" cross helicity whose sign indicates inward or outward propagating waves. They found that the rectified cross helicity changes sign inside switchbacks, while the normal cross helicity does not. Consequently, we can conclude that all the waves observed in and outside switchbacks are outwardly propagating modes, likely related to the quiescent solar wind of Dudok de Wit et al. ([2020](#)), and unrelated to the switchbacks that simply propagate through the quiescent background solar wind.

Figure 3 of Kasper et al. ([2019](#)) shows an example of a rather large switchback structure, lasting $\sim 105 + 325 + 30 = 460$ s. The initial $\sim 105$ s period (identified as a possible "transition region" by Kasper et al.) contains multiple large-amplitude radial magnetic field and velocity fluctuations that each exhibit large and rapid magnetic field rotations. An extended (325 s) less variable region of the switchback follows, with plasma characteristics quite different from the surrounding ambient solar wind. This, we suggest, is due to loop material propagating outwards as a fast mode magnetosonic structure, as we discuss below explicitly. We further show that as multiple strands of closely spaced open magnetic field and loop magnetic fields experience interchange reconnection events, PSP should observe a similar complex switchback structure higher in the corona.

The purpose of this paper is to provide an admittedly idealized linear quantitative theory describing the propagation of a structure that resembles a switchback based on the generation mechanism described above, i.e., we derive a linear wave equation describing the evolution of S-shaped and other less extreme structures as they propagate through the inhomogeneous solar corona. This allows us to examine the extent to which the inhomogeneity of the coronal flow modifies the structure and properties of the initial magnetic field deflection. We show that despite the linear and slowly varying background assumptions, the basic properties of the model are surprisingly consistent qualitatively and quantitatively with those of observed switchbacks. The extension to a nonlinear model will be described elsewhere. We show that the derived evolution equation admits an analytic multidimensional, time-dependent solution.

The model, derivation of the linear evolution equation, and solutions are presented in the following section, after which a summary is provided.

## 2. Model and Results

Let us assume that the standard MHD equations are a suitable model for the solar corona in the region ($\sim 6\,R_\odot$) where one might expect an interchange reconnection of the sort illustrated in Figure [3](#) to occur. Hence,

$$\frac{\partial \rho}{\partial t} + \nabla \cdot \rho \boldsymbol{U} = 0; \tag{1}$$

$$\rho \left( \frac{\partial \boldsymbol{U}}{\partial t} + \boldsymbol{U} \cdot \nabla \boldsymbol{U} \right) = -\nabla P + \frac{1}{\mu_0} (\nabla \times \boldsymbol{B}) \times \boldsymbol{B}; \tag{2}$$

$$\frac{\partial \boldsymbol{B}}{\partial t} = \nabla \times (\boldsymbol{U} \times \boldsymbol{B}); \tag{3}$$

$$\frac{\partial P}{\partial t} + \boldsymbol{U} \cdot \nabla P + \gamma P \nabla \cdot \boldsymbol{U} = 0; \tag{4}$$

$$\nabla \cdot \boldsymbol{B} = 0, \tag{5}$$

where $\Psi \equiv (\rho,\ P, \boldsymbol{U}, \boldsymbol{B})$ is the state MHD eigenvector comprising the mass density, pressure, velocity, and magnetic field, $\gamma$ is the adiabatic index, and $\mu_0$ the permeability of free space. We assume an idealized inhomogeneous steady spherically symmetric background, varying only in the radial coordinate $r$ such that $\rho_0\ (r)$, $P_0(r)$, $\boldsymbol{U}_0 = U_0(r)\hat{\boldsymbol{r}}$, $\boldsymbol{B}_0(r) = B_0(r)\hat{\boldsymbol{r}}$ satisfy

$$r^2 \rho_0(r) U_0(r) = r_0^2 \rho_0(r_0) U_0(r_0); \tag{6}$$

$$B_0(r) = \frac{r_0^2}{r^2} B_0(r_0); \tag{7}$$

$$P_0(r) = P_0(r_0) \left( \frac{\rho_0(r)}{\rho_0(r_0)} \right)^{\gamma}, \tag{8}$$

where $r_0$ is a suitable reference distance. For the solutions below, we make the simplifying assumption that $U_0 \simeq constant$. Illustrated in Figure [4](#) is a plot of a turbulence-driven solar wind model (Zank et al. [2018](#); Adhikari et al. [2020a](#), [2020b](#)), showing that the coronal flow becomes supersonic at $\sim 2\,R_\odot$, after which the radial speed is essentially constant. The Alfvén speed is plotted too for the radial magnetic field (Equation ([7](#))), and the solar wind, although supersonic, remains sub-Alfvénic until $\sim 11\,R_\odot$ (the "Alfvén surface"). Hence, (1) it is reasonable to make the simplifying assumption that $U_0$ is constant, and (2) of the two oppositely propagating magnetosonic structures launched by a interchange
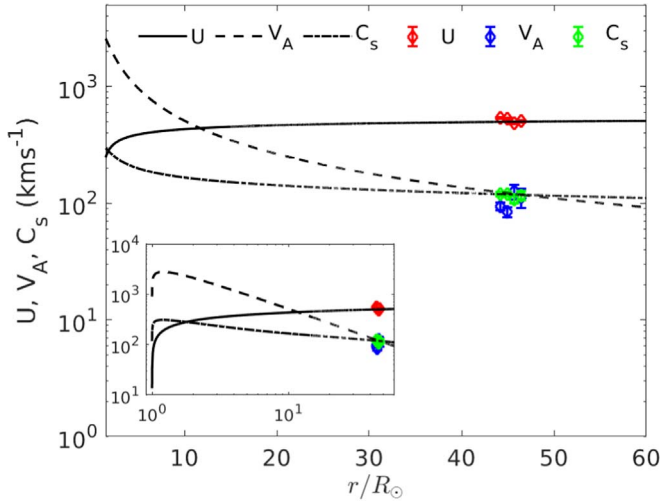
**Figure 4.** Plot of the solar wind speed (solid curve), the Alfvén speed (dashed curve), and the sound speed (dashed–dotted–dashed curve) based on the coronal heating and solar wind model of Adhikari et al. (2020a). The red, blue, and green symbols correspond to the observed solar wind speed, Alfvén speed, and sound speed, respectively, observed during the first encounter by PSP. The plot shows that the solar wind speed changes very slowly and is approximately constant after $\sim 4\,R_\odot$ and that, although supersonic, is sub-Alfvénic within $\sim 11$–$12\,R_\odot$.

reconnection event at $\sim 6\,R_\odot$, only one will propagate outwards since the other propagates toward the solar surface and is not advected outward. Figure 4 illustrates that the solar wind speed, sound speed, and Alfvén speed observed by PSP on the first encounter are consistent with the model. The parameters that we adopt in modeling the switchbacks are consistent with both the observed solar wind and the solar wind model between $\sim 6$ and $50\,R_\odot$.

An important quantity in the analysis below is the value of the plasma beta $\beta_{p0} = P_0/(B_0^2/2\mu_0) = (2/\gamma)C_0^2/V_{A0}^2$, which is small in the solar corona ($C_0^2 = \gamma P_0/\rho_0$ and $V_{A0}^2 = B_0^2/(\mu_0\rho_0)$ are the square of the sound and Alfvén speed, respectively). As can be seen in Figure 1, the proton plasma beta has typical values of $\sim 0.2$ already during the first of the PSP encounters, and these values can be expected to decrease as PSP draws ever closer to the solar surface.

To investigate the propagation of a disturbance initiated by an interchange reconnection event, we consider here a linear theory. Accordingly, we linearize the MHD Equations (1)–(5) about the nonuniform background (6)–(8) and assume that $U_0(r)$ is constant. We also translate the linearized equations into the background solar wind frame, allowing us to replace the convective derivative $\partial/\partial t + U_0 \cdot \nabla \mapsto \partial/\partial t'$. For notational convenience, we drop the prime henceforth and now let $\psi = (\rho, p, u, B)$ denote the linearized variables. In the solar wind frame, we therefore have

$$\frac{\partial \rho}{\partial t} + \rho_0(r)\nabla \cdot u + u \cdot \nabla P_0(r) + \rho \nabla \cdot U_0(r) = 0; \quad (9)$$

$$\frac{\partial u}{\partial t} = -\frac{1}{\rho_0}\nabla p + \frac{1}{\mu_0 \rho_0}(\nabla \times B) \times B_0(r); \quad (10)$$

$$\frac{\partial B}{\partial t} = B_0 \cdot \nabla u - B_0(r)(\nabla \cdot u) - u \cdot \nabla B_0(r) - B\nabla \cdot U_0(r); \quad (11)$$

$$\frac{\partial p}{\partial t} + \gamma P_0(r)\nabla \cdot u + u \cdot \nabla P_0(r) + \gamma p\nabla \cdot U_0(r) = 0; \quad (12)$$

$$\nabla \cdot B = 0. \quad (13)$$

The background solar wind flow has characteristic length $L$ and time $T$ scales that far exceed the spatial and temporal scales associated with the impulsive disturbance initiated by the reconnection event and the observed switchbacks. Hence, following the standard Jeffreys–Wentzel–Kramers–Brillouin (JWKB) approach, we assume that the MHD variables exhibit a slowly varying and a rapidly varying dependence on large and small scales, i.e., we can define fast and slow timescales and short and long wavelength scales via

$$\begin{aligned}\tau &= t/\varepsilon \\ t &= t\end{aligned} \quad \text{and} \quad \begin{aligned}\xi &= x/\varepsilon \\ x &= x\end{aligned},$$

where $\varepsilon \sim O(\ell/L)$ and $\ell$ is a characteristic spatial scale of the disturbance. We can expand the MHD variables as

$$\psi = \psi_1(\xi, \tau; x, t) + \varepsilon\psi_2(\xi, \tau; x, t) + \cdots. \quad (14)$$

At $O(1/\varepsilon)$, using $\partial_t \mapsto \varepsilon^{-1}\partial_\tau + \partial_t$ and $\nabla \mapsto \varepsilon^{-1}\nabla_\xi + \nabla_X$, we obtain

$$\frac{\partial \rho_1}{\partial \tau} + \rho_0 \nabla_\xi \cdot u_1 = 0; \quad (15)$$

$$\frac{\partial u_1}{\partial \tau} = -\frac{1}{\rho_0}\nabla_\xi p_1 + \frac{1}{\mu_0 \rho_0}(\nabla_\xi \times B_1) \times B_0; \quad (16)$$

$$\frac{\partial B_1}{\partial \tau} = B_0 \cdot \nabla_\xi u_1 - B_0 \nabla_\xi \cdot u_1; \quad (17)$$

$$\frac{\partial p_1}{\partial \tau} = -\gamma P_0 \nabla_\xi \cdot u_1; \quad (18)$$

$$\nabla_\xi \cdot B_1 = 0, \quad (19)$$

where $\nabla_\xi$ denotes the gradient operator with respect to the $\xi$ coordinate (below, we use $\nabla_X$ for the corresponding $x$ coordinate). By introducing $\Delta_1 \equiv \nabla_\xi \cdot u_1$, Equations (15)–(19) can be expressed as the wave equation (Lighthill 1960; Zank et al. 2017),

$$\frac{\partial^4 \Delta_1}{\partial \tau^4} + (V_{A0}^2 + C_0^2)\nabla_\xi^2\frac{\partial^2 \Delta_1}{\partial \tau^2} + C_0^2 V_{A0}^2 \nabla_\xi^2\frac{\partial^2 \Delta_1}{\partial \xi_x^2} = 0, \quad (20)$$

where locally the mean magnetic field $B_0$ is aligned with the $x$-direction (hence $\xi_x$ above). Equation (20) can be solved using a spatial-temporal Fourier transform (e.g., Adam 2017), corresponding to a superposition of normal modes

$$\Delta_1(\xi, \tau; x, t) = \bar{\Delta}_1(x, t)e^{i\varphi(\xi,\tau)}, \quad (21)$$

where

$$\frac{\partial \varphi}{\partial \tau} = \omega, \quad \nabla_\xi \varphi = -k, \quad (22)$$

expresses that the ray equation $k_t + \nabla_\xi \omega = 0$ is satisfied. This yields of course the standard dispersion relation for fast and slow magnetosonic modes with phase speeds

$V_{f,s} \equiv V_{\pm} = \omega/k^2 \boldsymbol{k}, k = |\boldsymbol{k}|$, where

$$\omega^4 - (V_{A0}^2 + C_0^2)k^2\omega^2 + C_0^2 V_{A0}^2 k^2 k_x^2 = 0. \quad (23)$$

The next order expansion $O(1)$ yields

$$\frac{\partial \rho_2}{\partial \tau} + \rho_0 \nabla_{\xi} \cdot \boldsymbol{u}_2$$
$$= -\frac{\partial \rho_1}{\partial t} - \rho_0 \nabla_X \cdot \boldsymbol{u}_1 - \boldsymbol{u}_1 \cdot \nabla_X \rho_0 - \rho_1 \nabla_X U; \quad (24)$$

$$\frac{\partial \boldsymbol{u}_2}{\partial \tau} + \frac{1}{\rho_0} \nabla_{\xi} p_2 - \frac{1}{\mu_0 \rho_0} (\nabla_{\xi} \times \boldsymbol{B}_2) \times \boldsymbol{B}_0$$
$$= -\frac{\partial \boldsymbol{u}_1}{\partial t} - \frac{1}{\rho_0} \nabla_X p_1 + \frac{1}{\mu_0 \rho_0} [(\nabla_X \times \boldsymbol{B}_1) \times \boldsymbol{B}_0$$
$$+ (\nabla_X \times \boldsymbol{B}_0) \times \boldsymbol{B}_1]; \quad (25)$$

$$\frac{\partial \boldsymbol{B}_2}{\partial \tau} - \boldsymbol{B}_0 \cdot \nabla_{\xi} \boldsymbol{u}_2 + \boldsymbol{B}_0 \nabla_{\xi} \cdot \boldsymbol{u}_2$$
$$= -\frac{\partial \boldsymbol{B}_1}{\partial t} + \boldsymbol{B}_0 \cdot \nabla_X \boldsymbol{u}_1 - \boldsymbol{B}_0 \nabla_X \cdot \boldsymbol{u}_1$$
$$- \boldsymbol{u}_1 \cdot \nabla_X \boldsymbol{B}_0 - \boldsymbol{B}_1 \nabla_X \cdot \boldsymbol{U}_0; \quad (26)$$

$$\frac{\partial p_2}{\partial \tau} + \gamma P_0 \nabla_{\xi} \cdot \boldsymbol{u}_2$$
$$= -\frac{\partial p_1}{\partial t} - \gamma P_0 \nabla_X \cdot \boldsymbol{u}_1 - \boldsymbol{u}_1 \cdot \nabla_X P_0 - \gamma p_1 \nabla_X \cdot \boldsymbol{U}_0; \quad (27)$$

$$\nabla_{\xi} \cdot \boldsymbol{B}_2 = -\nabla_X \cdot \boldsymbol{B}_1. \quad (28)$$

Corresponding to Equation (21) and the expansion expansion equation, Equation (14), we substitute $\psi_{1,2}(\xi, \tau; \boldsymbol{x}, t) = \bar{\psi}_{1,2}(\boldsymbol{x}, t) \exp i\varphi(\xi, \tau)$ into Equations (24)–(28). In so doing, one can eliminate the $\psi_2$ variables via the dispersion relation, Equation (23), leaving an equation (the secularity condition) that describes the evolution of the $\bar{\psi}_1$ variables only in the slowly varying, long spatial scale coordinates.

The simplification of the secularity condition is quite formidable but is greatly aided by exploiting the small plasma beta condition $\beta_{p0} \ll 1$ in the solar corona. In this case, it is evident that the wave equation, Equation (20), reduces to

$$\frac{\partial^2 \Delta_1}{\partial \tau^2} - V_{A0}^2 \nabla_{\xi}^2 \Delta_1 = 0. \quad (29)$$

Thus, to leading order, the fast magnetosonic mode propagates at approximately the Alfvén speed[4] This is *not* an Alfvén wave as it neither propagates exclusively along the magnetic field line nor is it incompressible. In the $\beta_{p0} \ll 1$ limit, the fluctuating plasma variables are related to the fluctuating magnetic field $\bar{B}_{x1}$ (where x is aligned with the local magnetic field) through the eigenrelations listed in the Appendix. On utilizing the eigenvalue relations, we obtain a wave equation that describes the inward and outward propagation of $\bar{B}_{x1}$

through the inhomogeneous corona,

$$\frac{\partial \bar{B}_{x1}}{\partial t} \pm \frac{V_{A0}\boldsymbol{k}}{k} \cdot \nabla_X \bar{B}_{x1} = -\mathcal{D}\bar{B}_{x1}, \quad (30)$$

where the decay term $\mathcal{D} \simeq (U_0 + V_{A0}/2)/r$ is due to coronal expansion and is expressed in spherical coordinates. In Equation (30), the directional derivative term is simply the phase or wave propagation speed (since recall that $\boldsymbol{V}_p = \omega \boldsymbol{k}/k^2 = \pm(V_{A0}k/k^2)\boldsymbol{k} = \pm V_{A0}\boldsymbol{k}/k$). The vector $\boldsymbol{k}$ here corresponds to the initial direction in which the wave was launched by the interchange reconnection event, i.e., $\boldsymbol{k} = k(\cos \chi, \sin \chi \cos \lambda, \sin \chi \sin \lambda) \equiv k\hat{\boldsymbol{n}}$ since $\boldsymbol{B}_0 \| \hat{\boldsymbol{x}}$.

We wish to express Equation (30) in spherical coordinates ($r$, $\theta$, $\phi$) but the $\phi$ behavior is not of great interest. We gyrophase the average $\bar{B}_{x1}$ and introduce a new coordinate,

$$n = r \sin \theta \geqslant 0. \quad (31)$$

Kasper et al. (2019) found that switchbacks propagate approximately radially outwards, which is consistent with a source located in the sub-Alfvénic region of the corona. Hence, despite $0 \leqslant \theta \leqslant \pi$, $\theta$ is restricted to somewhat small angles, which allows us to approximate $\partial/\partial\theta = r\sqrt{1 - n^2/r^2}\partial/\partial n \simeq r(1 - n^2/2r^2)\partial/\partial n \simeq r\partial/\partial n$, provided that $n^2/2r^2 \ll 1$, after choosing the positive root for outward propagation. The linear evolution equation for a switchback can then be written as

$$\frac{\partial \bar{B}_{x1}}{\partial t} + aV_{A0}\frac{\partial \bar{B}_{x1}}{\partial r} + bV_{A0}\frac{\partial \bar{B}_{x1}}{\partial n} = -\mathcal{D}\bar{B}_{x1}, \quad (32)$$

where $(a, b) = (\cos \chi, \sin \chi \cos \lambda)$, $0 < \chi < \pi/2$, $0 < \lambda < 2\pi$ are coefficients of the directional derivatives.

Equation (32) can be solved as an initial value problem (IVP) for the radial component of the magnetic field perturbation by prescribing

$$\bar{B}_{x1}(r, n, t = 0) = f(r, n), \quad r > 0, n > 0, \quad (33)$$

at some location ($r,n$), i.e., at a prescribed height and over a specified region. The general solution of the IVP, Equations (32) and (33), is

$$\bar{B}_{x1}(r, n, t) = f(\kappa, \eta)\left(\frac{\kappa}{r}\right)^{1/2a}\exp\left[-\frac{U_0}{aV_{A0}^0}\left(\frac{r - \kappa}{r_0}\right)\right];$$
$$\kappa = r\left(1 - 2aV_{A0}^0 r_0 \frac{t}{r^2}\right)^{1/2}; \quad \eta = n - \frac{b}{a}(r - \kappa), \quad (34)$$

where $r_0$ is a reference height and $V_{A0}^0 \equiv V_{A0}(r = r_0)$. The full solution for the radial field as a switchback propagates up through the corona is therefore $B_r(r, \theta, t) = B_0(r) + B_{x1}(r, n, t)$.

Recall that we assume that the interchange reconnection event essentially expels a "blob" of plasma into the expanding solar coronal wind, most likely with a density and temperature reflecting loop material and a speed roughly that of the local Alfvén speed in the frame of the solar wind, and in a direction that is not necessarily radial. Because the interchange reconnection occurs between radial open magnetic field line and non-radial loop magnetic field, the initial radial and transverse magnetic fields will be strongly perturbed. The expelled blob of plasma will be advected in the background

---

[4] Recall that in the low plasma beta limit, the slow mode propagation speed is approximately $V_s \simeq V_{A0}\sqrt{\gamma\beta_{p0}/2}\cos\theta \ll V_{A0}$ (Zank et al. 2019). Given this propagation speed, it is unlikely that a switchback is a slow magnetosonic structure. Moreover, a more rapidly propagating fast mode excited by the perturbed magnetic field would effectively straighten out any initial S-shaped structure and the subsequent slow mode structure would not exhibit large magnetic field deflections.
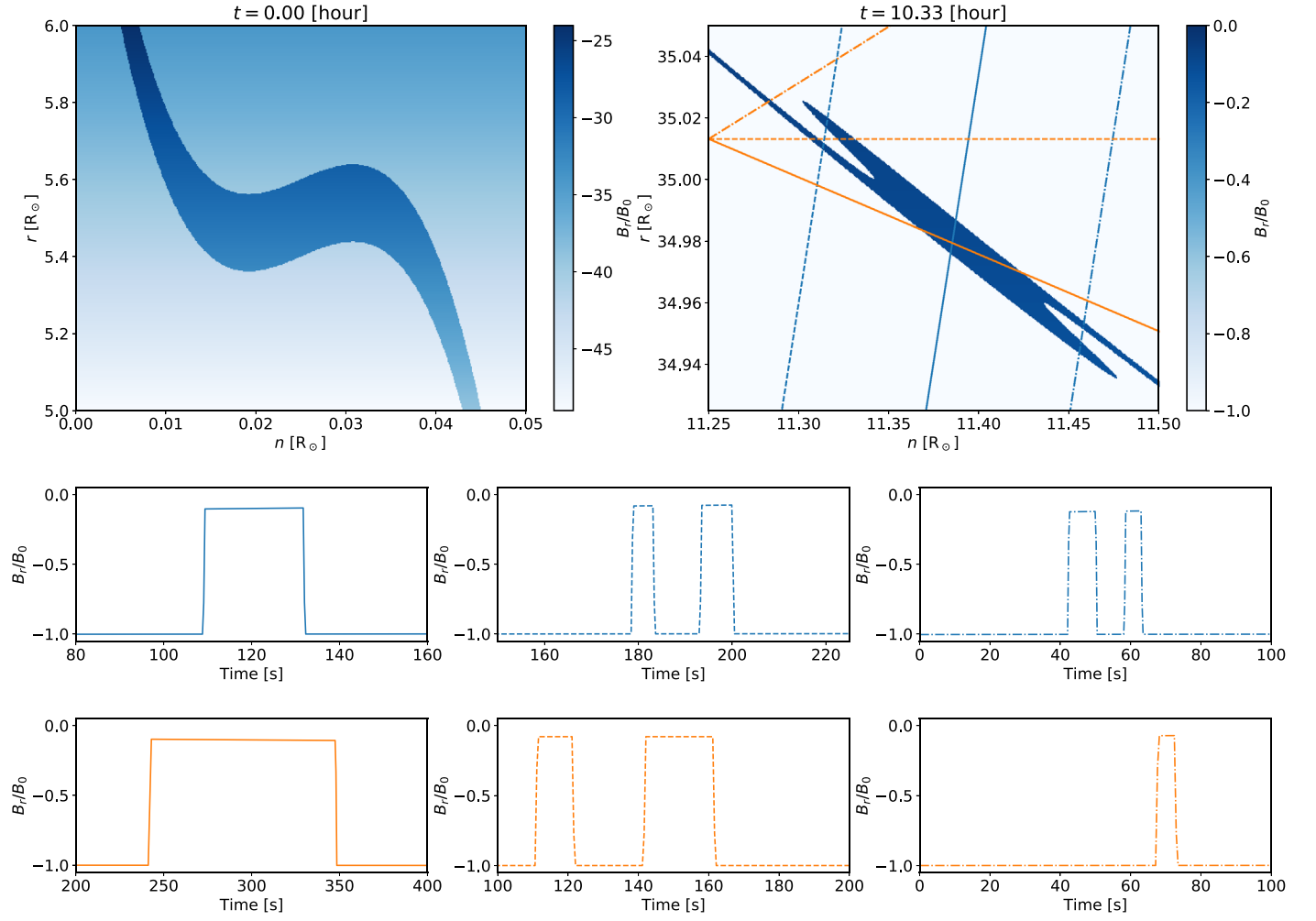
**Figure 5.** Top left: the initial radial magnetic field component of the switchback in the $(r,n)$-plane generated by interchange reconnection between an open magnetic field region and a large loop (see Figure 3) that extended to approximately 5.7 $R_\odot$. The color denotes the magnetic field intensity, where the background strength is given by Equation (7). Top right: snapshot of the propagating switchback about 9.7 h after the interchange reconnection event. The various lines through the figure correspond to hypothetical PSP trajectories. Middle and bottom panels: 1D time series of the magnetic field corresponding to each of the possible trajectories. The curve type and color corresponds to a trajectory shown in the top right panel.

flow and propagate at a characteristic speed consistent with the fastest wave mode (since it is not a shock). In the low plasma beta corona, this is essentially the Alfvén speed. This is obviously neither an Alfvén wave nor a fast magnetosonic wave since the initial plasma and magnetic field data are almost certainly not related via the eigenrelations of either the Alfvén or fast magnetosonic modes. Instead, this is an IVP governed by either (in the linear approximation—discussed further below) an Alfvén or fast magnetosonic propagator with the subsequent evolution of the initial state governed by the relevant eignerelations. However, the evolving and eventual state is not determined by the simple eigenrelations of either— the state is governed by the initial data. Consequently, switchbacks are not simple linear waves, neither Alfvén nor fast mode, but instead a complex structure propagating at the fast magnetosonic speed in a low plasma beta environment. Switchbacks propagate at the fast mode speed and have compressible and field-aligned magnetic field and velocity components, which is consistent with magnetosonic structures and not Alfvénic structures, and they are certainly not simple linear fast mode waves.

Simple initial conditions for a field-reversal form of switchback are a finite length, finite width box function on a

perturbed magnetic field curve defined by a cubic such as $f(r, n) = 1$ if $|r - r_1 = c (n - n_1)(n - n_2)(n - n_3)| < d$ and $0$ elsewhere for an initial S-shaped structure, or $f(r, n) = 1$ if $|r - r_1 = c (n - n_1)(n^2 + n_2)| < d$ and $0$ elsewhere for an initial non-S-shaped structure, with constants $c$, $d$, and $n_i$.

The top left panel of Figure 5 is a 2D plot of an initial state of the radial magnetic field component using a finite length, finite width box car function. The strength of the perturbation is given by color and the background is given by the mean radial magnetic field (Equation (7)). The pulse is launched at a height of 5.7 $R_\odot$ and the initial state then evolves according to Equation (34) up to a height of 35 $R_\odot$. The switchback evolves quite significantly in structure, becoming much more compressed and exhibiting a more extreme reversal in the magnetic field as it propagates into the higher corona. A time series of what PSP might observe were it to pass through different sections of the switchback is illustrated by the various curves in the middle and bottom panels of Figure 5. Here we used the switchback speed, the background solar wind advection speed, and the PSP speed to create the time series. Evidently, if one passes through the center or main body of the switchback, a single enhancement or pulse in the magnetic field will be observed, much like the example seen shortly after 11:43 or
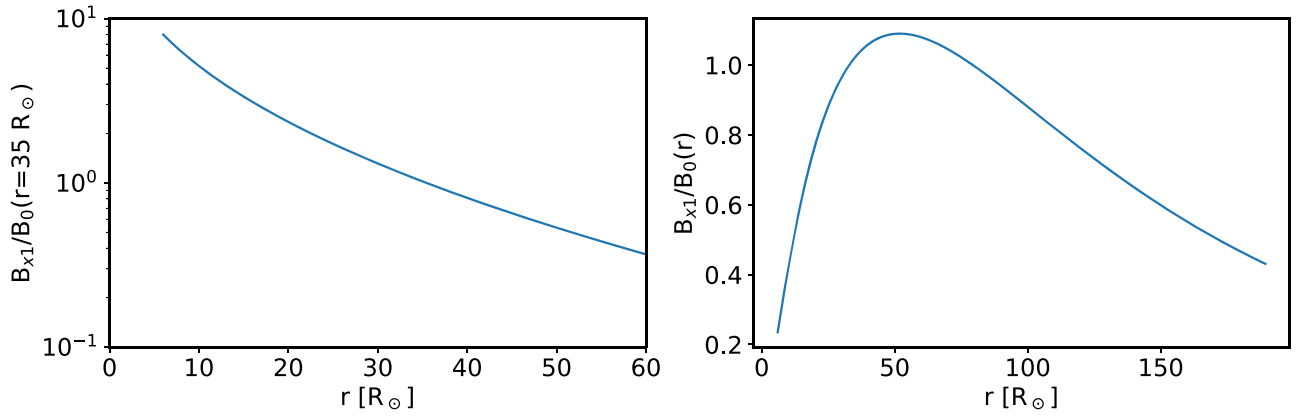
**Figure 6.** Left: decay of the switchback magnetic field amplitude $B_{x1}$ normalized to $B_0$ ($r = r_0$) ($r_0 = 35\,R_\odot$) from ∼6–60 $R_\odot$ for the example shown in Figure 5. Both the switchback propagation speed and advection are included in the decay rate calculation and $r$ refers to heliocentric distance. Right: plot of the decay of the switchback magnetic field amplitude $B_{x1}$ normalized to the local mean magnetic field $B_0(r)$. This plot identifies the region over which the "linear" analysis is approximately valid.

some of the other single pulses seen at later times in Figure 1. PSP will observe that the magnetic field reverses itself twice, i.e., has an S-shaped structure, within ∼20 s if one adopts the solid blue line trajectory, for example. The thickness of the spatial structure at ∼35 $R_\odot$ is about 0.01$R_\odot$.

If instead PSP happened to pass through the flanks of the switchback, this simple configuration would result in PSP observing a pair of closely spaced structures with a field reversal in one that is adjacent to another part that is oppositely oriented and uni-directional. The bottom panel shows time series for alternate trajectories were PSP to pass more laterally through a switchback. These possible 1D structures resemble those of the middle panel, which used an encounter 1 PSP trajectory. The closely spaced switchback structures at about 12:20, possibly just before 20:20, and just before 21:20 in Figure 1 resemble the double-humped structure of the 1D times series of Figure 5.

The color bar of the 2D switchback plots in Figure 5 reveals that the amplitude of the switchback decreased markedly in propagating from ∼6–35 $R_\odot$. This is due to the diverging solar wind flow attenuating the switchback as it propagates into the solar wind, and the right-hand side of Equation (32) $\mathcal{D}$ determines the rate at which the switchback weakens. Evidently, $\mathcal{D}$ is dominated by the velocity divergence that is proportional to $r^{-1}$ rather than the $r^{-2}$ divergence of the Alfvén speed. Plotted in Figure 6 (left) is the computed absolute decrease in the radial magnetic field amplitude with heliocentric distance, normalized to the ambient magnetic field at 35 $R_\odot$. The amplitude of the switchback decreases quite significantly by more than an order of magnitude over ∼60 $R_\odot$. The right plot shows $B_{x1}/B_0(r)$, where now the normalization varies locally with heliocentric distance $r$ since $B_0(r)$ is governed by Equation (7). Until ∼50 $R_\odot$, the amplitude of the switchback relative to the local or quiescent mean magnetic field (which is $\propto r^{-2}$) increases. Thereafter, the relative amplitude decreases. However, for $r < 40\,R_\odot$, $B_{x1}/B_0(r) < 1$, and the linear approximation used here, while not ideal, is at least reasonable. We show below an explicit comparison of the observed 11:43:45–11:45, 2018 November 6 switchback (Figure 2) and the theoretical model. The rather accurate comparison supports the idea that the linear approximation is surprisingly reasonable. This may be because the structure spends most of its propagation time satisfying $B_{x1}/B_0(r) < 1$. We suspect that this may account for the

unreasonable effectiveness of the model. At larger distances, a background magnetic field that includes the azimuthal component is necessary.

In Figure 7, we plot the plasma variables for one of the three 1D cuts that correspond to the PSP trajectories shown in Figure 5 (top right; the orange solid line). Besides the initial condition for $B_{x1}$, initial conditions for the remaining plasma variables should be assigned to the initial structure. These are tabulated in Table 1. The evolution of these quantities is then tracked via the eigenrelations listed in the Appendix. In choosing the initial plasma data, we assume that this corresponds to the simultaneous incorporation of loop plasma into the initial switchback structure. Since the loop plasma is typically hotter, especially for the larger loops (e.g., Feldman et al. 1999), and correspondingly more tenuous than the ambient coronal plasma, we assume that the plasma in the initial switchback structure has a higher temperature and lower number density than in the surrounding ambient plasma. We assume that the injection of the plasma blob from the reconnection event has a characteristic speed corresponding approximately to the local Alfvén speed, and that the initial propagation direction of the plasma parcel does not necessarily follow the radial direction. Furthermore, because the reconnection event occurs between open approximately radial magnetic field and non-radial loop magnetic field, we expect that the transverse magnetic field is also perturbed initially.

Figure 7 is a detailed comparison of the theoretical model ( i.e., the solution, Equation (34), with the switchback observed between at 11:43:45 and 11:45:35, 2018 November 6, plotted in the same normalized format as Figure 2 in the ordering and layout of the magnetic field and plasma variables, but without $\theta_B$. All quantities are normalized to the background or ambient state at 35 $R_\odot$ just ahead of the switchback. The panels correspond to PSP following a trajectory (Figure 5, right top) through the main body of the switchback. The solid red and blue curves correspond to PSP observations and the dashed red and blue curves to the same quantities for the theoretical model. The time series are plotted for the radial and transverse magnetic fields together with the corresponding velocity vector components on the same panels. The density and temperature, and thermal and magnetic pressure are each plotted in the panels that follow. Please note the scaling on the left and right ordinates is different. Finally, the plasma beta is plotted on the bottom row.
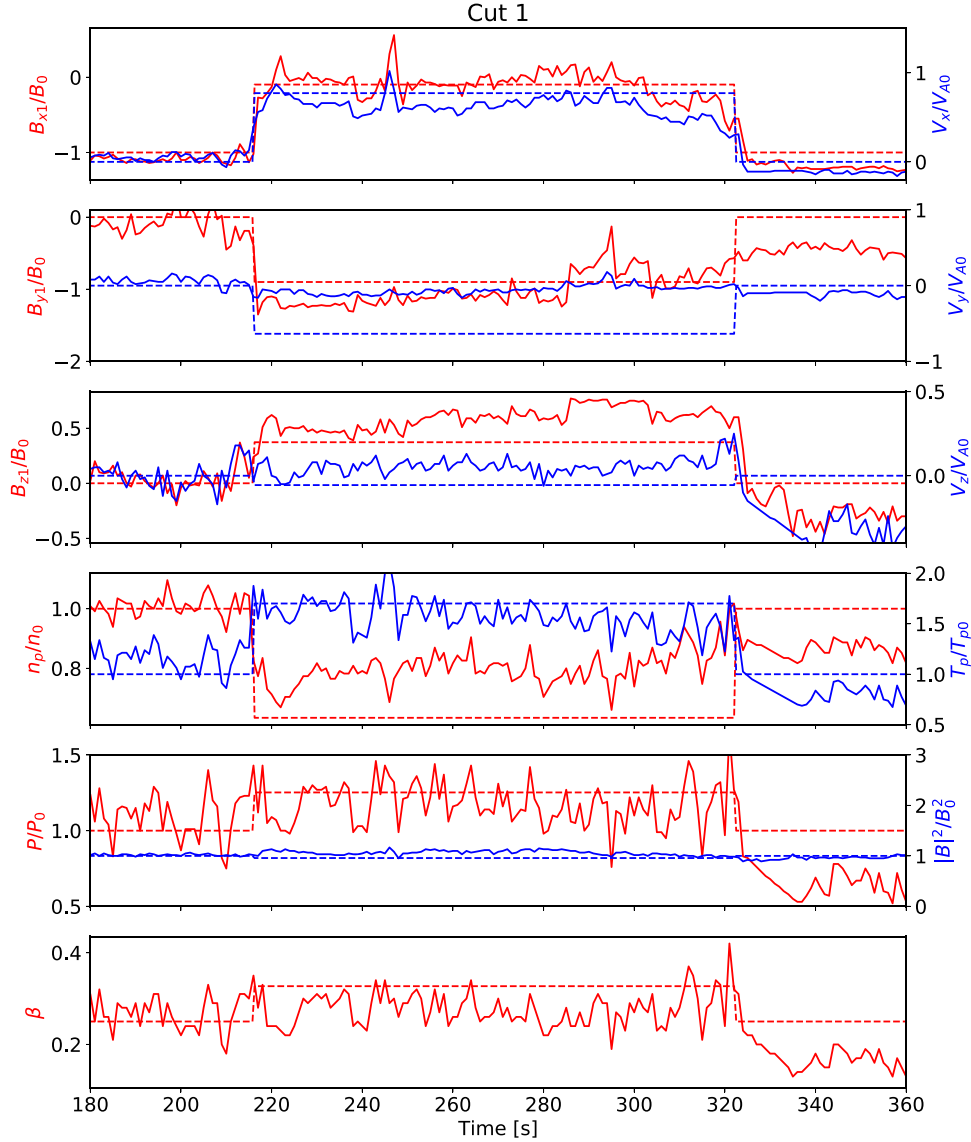
**Figure 7.** Comparison of model solutions and the switchback observed between at 11:43:45 and 11:45:35, 2018 November 6, plotted in the same normalized format as Figure 2 showing the normalized magnetic field and plasma variables, including the plasma beta, plotted as a time series. The colored solid and dashed lines depict the corresponding observations and model, respectively.

The modeled and observed single hump switchback are nicely consistent in the radial magnetic field ($B_{x1}/B_0$) increase and the radial velocity increase, both of which represent fast magnetosonic signatures and not Alfvénic signatures. The modeled and observed transverse magnetic field $B_{y1}/B_0$ decrease consistently across the switchback but the predicted decrease in the transverse velocity $u_{y1}/V_{A0}$ is larger than that observed. The modeled and observed normal magnetic field $B_{z1}/B_0$ and velocity $u_{z1}/V_{A0}$ components are in good accord, as are the modeled and observed proton temperature $T_p/T_{p0}$, pressure $P/P_0$, and plasma beta. The observed and modeled proton density $n_p/n_0$ are very similar too, although the predicted density is fractionally smaller than observed. Finally, we see that the magnetic pressure through the switchback is essentially constant in both the observations and model. As illustrated in Figure 5 (top right panel), the body of the switchback presented in Figure 7 possesses an S-shaped structure. In essence, the comparison allows us to probe the

conditions shortly after the interchange reconnection event that created the switchback low in the corona.

We comment that the properties of the magnetic and plasma variables shown in Figure 7 are similar to the range of properties, quantitatively and qualitatively, exhibited by the switchbacks identified by the gray shading in Figure 1. This includes the switchback plasma beta that is seen to increase and decrease modestly compared to the background thermal plasma. A subsequent detailed comparison of the theory, i.e., Equation (34), with other observed switchback examples is warranted.

Finally, in Figure 8, we plot the magnetic field and plasma variables in the same format as Figure 7 for a PSP trajectory that passes through the trailing or leading region of a switchback, i.e., the flanks of a switchback, as illustrated in middle and right lower panels of Figure 5. In this case, one has a double-peaked switchback structure, as discussed above, and the same magnetic field and plasma properties hold for the double-peaked structure. In this case, two closely spaced (in

**Table 1**
Initial Background Values Inside the Switchback

| $u_{x,sb}/V_{A0}$ | $u_{y,sb}/V_{A0}$ | $u_{z,sb}/V_{A0}$ | $b_{y,sb}/B_0$ | $b_{z,sb}/B_0$ | $\rho_{sb}/\rho_0$ | $T_{sb}/T_0$ | $\chi$ | $\lambda$ |
|---|---|---|---|---|---|---|---|---|
| $\cos\chi$ | $\sin\chi\cos\lambda$ | $\sin\chi\sin\lambda$ | 0 | 0.5 | 1/3 | 1.5 | 45° | 5° |

this case, ~5 s separation) jets are present with the associated magnetic field reversals. It is conceivable that the complex forward and trailing sheath structure presented in Figure 3 of Kasper et al. (2019) is possibly due to PSP transitioning the flank regions of a switchback, such as the dashed and dotted line trajectories in Figure 5. Figure 1 appears to contain examples of pairs of closely spaced switchbacks.

Let us consider more closely the apparent clustering of switchbacks and the possibility, as suggested by some of the events in Figure 1, that switchbacks are not necessarily all simple, single jet, S-shaped magnetic field structures. Physically, we should not think of a "single magnetic field line" loop and open magnetic field but consider rather many strands of closely packed open magnetic and loop magnetic field lines (analogous to the many wires comprising telephone cable) that experience multiple interchange reconnection events over a short time that then initiates a series of closely spaced switchbacks. Figure 9 illustrates a complex of initially closely located switchback structures and shows their resulting evolution as they propagate collectively through the corona. By constructing a set of time series plots for several possible PSP trajectories, we can account for some of the more complex switchback events illustrated in Figure 1 and in Kasper et al. (2019).

Using the same format as Figure 5, the top left panel shows the initial state after a series of switchbacks of varying initial propagation directions and magnetic field orientations were created by multiple closely spaced interchange reconnection events. The top right panel shows the evolved complex after 10.33 h, illustrating that the clustering has persisted and become more complex. Many field reversals are effectively stacked close together. The middle row shows the radial magnetic field time series for three possible PSP trajectories. The leftmost of the middle row of panels shows an obvious central switchback structure, preceded and followed by narrow switchback structures. The middle panel of the row shows a less broad although discernible switchback, but now preceded and followed by numerous rapidly varying jets. This is very suggestive of a switchback shown in Figure 3 of Kasper et al. (2019), in which a transition region has multiple large-amplitude magnetic field and velocity fluctuations that each exhibit large and rapid magnetic field rotations. A quite different example is illustrated in the last panel of the row (the blue dashed line) where the time series shows no single broad structure, being instead a series of short-lived, small-scale switchbacks with a possible gap separating the two jet clusters. The bottom row of panels corresponds to the orange trajectories shown in the top right panel. Similar comments about the possible array of switchback structures apply to these solutions as well.

## 3. Conclusions

Switchbacks exhibit a power law in magnetic field deflections, which includes a small number of complete reversals, appear to be created in coronal regions well above the photosphere, and tend to aggregate or cluster (Dudok de Wit et al. 2020). Conceptually, we suggest that the origin of switchbacks is due to interchange magnetic reconnection between coronal loops and open magnetic field regions, as illustrated in Figure 3. Based on the observed compressible characteristics of switchbacks (a variable density, pressure, radial magnetic field, and radial velocity component, none of which is consistent with Alfvénic structures), we argue that a switchback is a compressible complex structure propagating at the fast magnetosonic speed through the low plasma beta corona, i.e., at approximately the Alfvén speed, at an angle to the mean magnetic field. We formulate a model of switchback structure and propagation using linear theory in a slowly varying background coronal plasma, deriving an evolution equation for the amplitude of the radial magnetic field component. An analytic solution describing the evolution of a switchback with arbitrary initial conditions is found and used to examine the properties of switchbacks in the corona. Our results are summarized as follows:

1. Interchange reconnection creates an initial magnetic field deflection and perturbation on reconfigured open magnetic field lines. The initial structure likely entrains loop plasma that is hotter and more tenuous than the ambient coronal plasma, and corresponds to a blob of plasma moving at approximately the Alfvén speed in a direction that is not necessarily radial. A possible test for the entrainment of loop plasma might be the compositional characteristics of the switchback plasma, which may be different from the ambient plasma.

2. The fast magnetosonic switchback propagates at approximately the Alfvén speed, decaying in absolute amplitude with increasing heliocentric distance, but increasing in amplitude relative to the local mean magnetic field strength until ~50 $R_\odot$. The relative amplitude remains <1 until at least 35 $R_\odot$, thereby providing some justification for the linear theory. The 3D structure of the initial switchback is largely preserved with increasing distance although becoming "tighter" and decreasing in spatial width from ~0.1 $R_\odot$ at ~6 $R_\odot$ to ~0.01 $R_\odot$ at 35 $R_\odot$ for the example we consider.

3. Depending on the relative orientation with which PSP flies through a simple single switchback, the model predicts that PSP would observe either a single structure or a closely spaced double hump or peak structure. The single structure corresponds to PSP flying through the main body of the switchback whereas the double-humped structure corresponds to PSP flying through the flank of a switchback. The double-peaked structure might comprise two magnetic field reversals or a reversal and an adjacent uni-directional magnetic field and both structures would be close together.

4. Besides the radial magnetic field of the switchback, the remaining magnetic field components and plasma variables can be computed. Specifically, we model the switchback observed on the first PSP encounter between at 11:43:45 and 11:45:35, 2018 November 6, and compare the model results to the observations. The velocity increases abruptly in going from the ambient
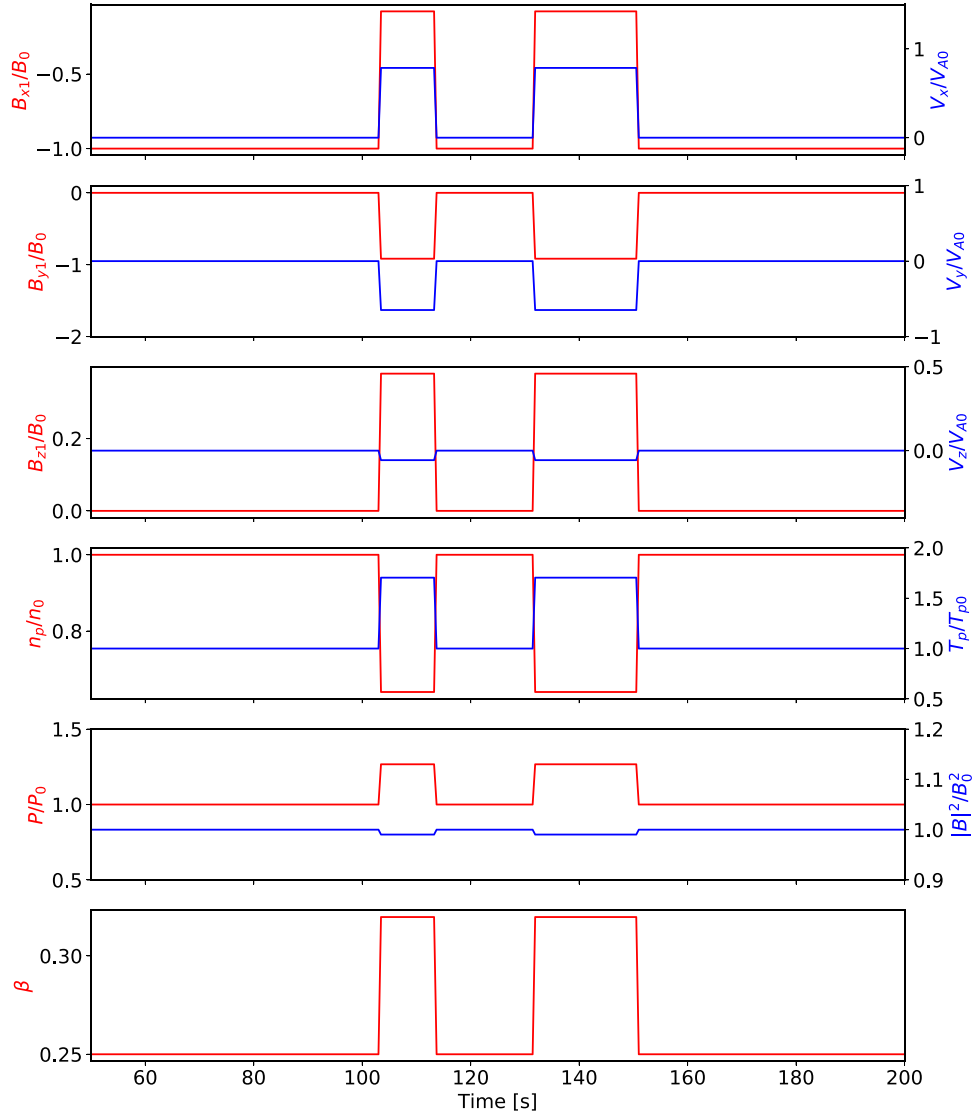
**Figure 8.** The magnetic field and plasma variables in the same format as Figure 7 for a PSP trajectory that passes through the trailing or leading region of a switchback, i.e., the flanks of a switchback, illustrating a possible double-peaked switchback structure.

plasma to the switchback (a "jet"), the switchback temperature and pressure are higher and the density lower than the surrounding ambient plasma, and the plasma beta increases modestly over the ambient value. These characteristics are both qualitatively and quantitatively in very good agreement with the observed example. Furthermore, the model results suggest that a more detailed comparison could reasonably be made with the other switchback examples presented in Figure 1.

5. Finally, to address both the aggregation or clustering of switchbacks (Dudok de Wit et al. 2020) and their sometimes complicated structure (e.g., our Figure 1 or Figure 3 of Kasper et al. 2019), we consider multiple closely spaced switchbacks created by interchange reconnection with numerous open and loop magnetic field lines. Their evolution yields a complex, highly aggregated group of switchbacks at e.g., $35\,R_\odot$. One hypothetical time series for a trajectory through an aggregate of switchbacks yields a sheath-like structure on either side of a broad box-like switchback structure. The sheaths contain numerous large-amplitude radial

magnetic field and velocity fluctuations that exhibit large and rapid deflections. Other example solutions correspond to many large-amplitude radial magnetic field and plasma fluctuations without a single identifiable broad switchback structure.

The model presented here, despite its relative simplicity, appears to capture the basic relations between the magnetic field and plasma variables, describes the field reversals and S-shaped structures, and the propagation characteristics. We emphasize that the observed switchback characteristics reflect the initial conditions at its time of formation by an interchange reconnection event. The subsequent evolution of these quantities is governed by the fast mode magnetosonic relations and not by Alfvénic relations. The model further appears to describe the sometimes complicated structures observed in and around switchbacks, this being a consequence of PSP flying through different parts of one or many switchbacks. The model offers considerable scope for validation against observations.
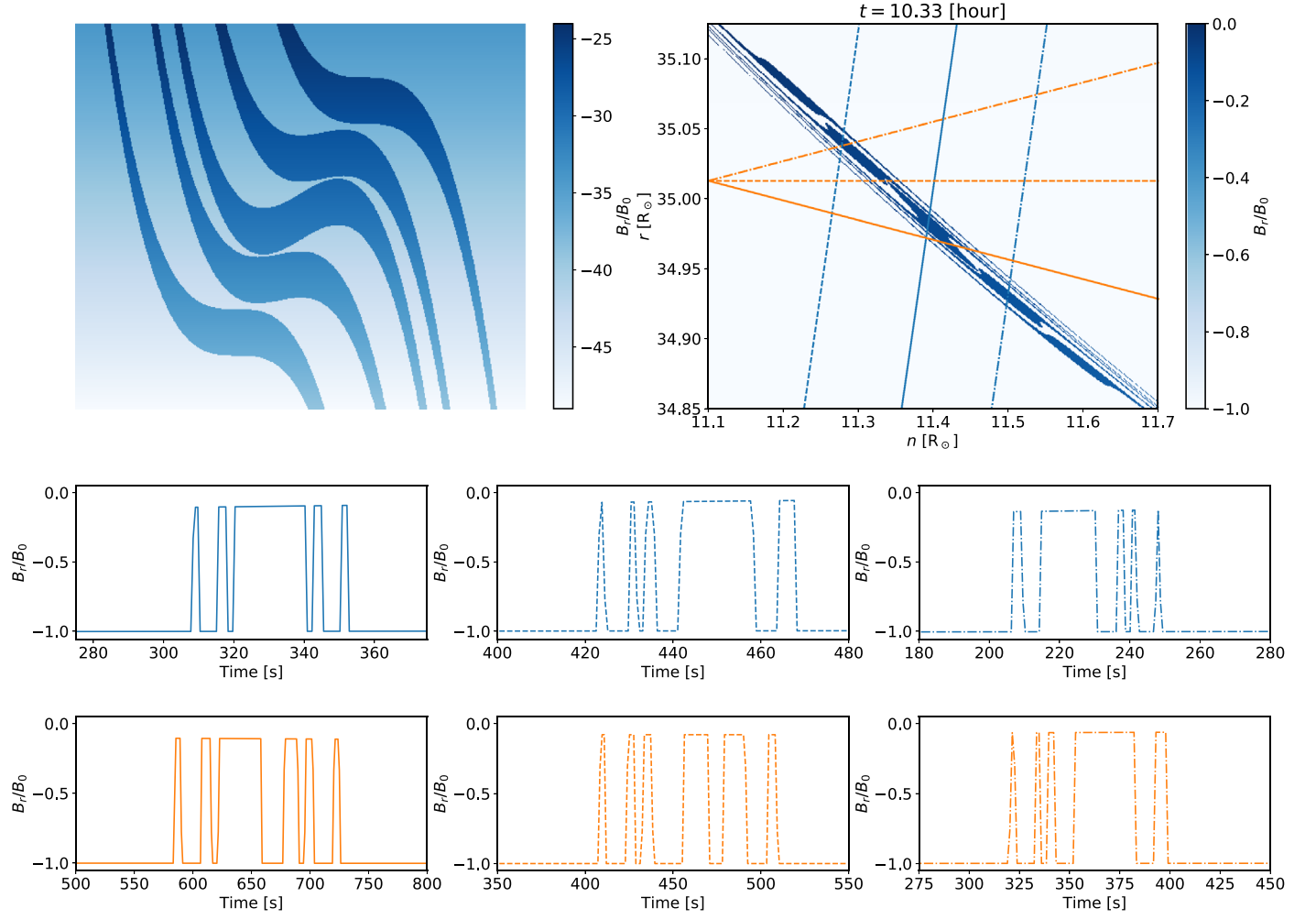
**Figure 9.** Evolution of a set of initially closely spaced switchbacks (top left) after 9.72 h (top right) in the same format as Figure 5. Three possible PSP trajectories are plotted in the top right panel (blue-dotted, solid, and dashed lines) together with three other potential trajectories (orange lines). Plotted in the middle row are panels of time series of the radial magnetic field $B_r$ corresponding to the possible PSP trajectories with the corresponding line types. The bottom row plots the corresponding time series of $B_r$ for the orange trajectories.

## Appendix
## Eigenrelations in the $\beta_{p0} \ll 1$ Limit

The eigenrelations relating the local fluctuating plasma variables to the fluctuating magnetic field in the plasma beta limit $\beta_{p0} \ll 1$ are listed:

$$\frac{\rho_1}{\rho_0} \simeq \frac{B_{x1}}{B_0}; \qquad \frac{p_1}{P_0} \simeq \gamma \frac{B_{x1}}{B_0}; \qquad u_{x1} \simeq \pm \frac{C_0^2}{V_{A0}} \cos\chi \frac{B_{x1}}{B_0};$$

$$u_{y1} \simeq \pm V_{A0} \frac{\cos\lambda}{\sin\chi} \frac{B_{x1}}{B_0}; \qquad u_{z1} \simeq \pm V_{A0} \frac{\sin\lambda}{\sin\chi} \frac{B_{x1}}{B_0};$$

$$\frac{T_1}{T_0} \simeq (\gamma - (1)) \frac{B_{x1}}{B_0};$$

$$B_{y1} \simeq -\frac{\cos\chi \cos\lambda}{\sin\chi} B_{x1}; \qquad B_{z1} \simeq -\frac{\cos\chi \sin\lambda}{\sin\chi} B_{x1}.$$

The pitch angle $\chi$ and gyrophase angle $\lambda$ correspond to the initial launch angles of the fluctuation after the interchange reconnection event.

## ORCID iDs

G. P. Zank ⦿ https://orcid.org/0000-0002-4642-6192
M. Nakanotani ⦿ https://orcid.org/0000-0002-7203-0730
L.-L. Zhao ⦿ https://orcid.org/0000-0002-4299-0490
L. Adhikari ⦿ https://orcid.org/0000-0003-1549-5256
J. Kasper ⦿ https://orcid.org/0000-0002-7077-930X

## References

Adam, J. A. 2017, Rays, Waves, and Scattering: Topics in Classical Mathematical Physics, Vol. 56 (Princeton, NJ: Princeton Univ. Press)
Adhikari, L., Zank, G., & Zhao, L.-L. 2020a, ApJ, 901, 102
Adhikari, L., Zank, G. P., Zhao, L. L., et al. 2020b, ApJS, 246, 38
Bale, S. D., Goetz, K., Harvey, P. R., et al. 2016, SSRv, 204, 49
Dudok de Wit, T., Krasnoselskikh, V. V., Bale, S. D., et al. 2020, ApJS, 246, 39
Feldman, U., Widing, K. G., & Warren, H. P. 1999, ApJ, 522, 1133
Fisk, L. A. 2003, JGRA, 108, 1157
Fisk, L. A. 2005, ApJ, 626, 563
Fisk, L. A., & Kasper, J. C. 2020, ApJL, 894, L4
Fisk, L. A., & Schwadron, N. A. 2001, ApJ, 560, 425
Fisk, L. A., Schwadron, N. A., & Zurbuchen, T. H. 1999, JGR, 104, 19765
Horbury, T. S., Forman, M., & Oughton, S. 2008, PhRvL, 101, 175005
Kasper, J. C., Abiad, R., Austin, G., et al. 2016, SSRv, 204, 131
Kasper, J. C., Bale, S. D., Belcher, J. W., et al. 2019, Natur, 576, 228
Landi, S., Hellinger, P., & Velli, M. 2006, GeoRL, 33, L14101

Lighthill, M. J. 1960, RSPTA, 252, 397
Matteini, L., Horbury, T. S., Neugebauer, M., & Goldstein, B. E. 2014, GeoRL, 41, 259
Matteini, L., Horbury, T. S., Pantellini, F., Velli, M., & Schwartz, S. J. 2015, ApJ, 802, 11
McManus, M. D., Bowen, T. A., Mallet, A., et al. 2020, ApJS, 246, 67
Tenerani, A., Velli, M., Matteini, L., et al. 2020, ApJS, 246, 32

Yamauchi, Y., Suess, S. T., Steinberg, J. T., & Sakurai, T. 2004, JGRA, 109, A03104
Zank, G. P., Adhikari, L., Hunana, P., et al. 2017, ApJ, 835, 147
Zank, G. P., Adhikari, L., Hunana, P., et al. 2018, ApJ, 854, 32
Zank, G. P., Nakanotani, M., & Webb, G. M. 2019, ApJ, 887, 116
Zhao, L. L., Zank, G. P., Adhikari, L., et al. 2020, ApJS, 246, 26